THE ASTROPHYSICAL JOURNAL, 494:773–782, 1998 February 20

A PHOTOMETRIC AND SPECTROPHOTOMETRIC STUDY OF MR CYGNI

A. P. LINNELL[1]
Department of Physics and Astronomy, Michigan State University, E. Lansing, MI 48824
P. B. ETZEL[2]
Department of Astronomy, San Diego State University, San Diego, CA 92182
I. HUBENY[3]
AURA/NOAO, NASA Goddard Space Flight Center, Code 681, Greenbelt, MD 20771
AND
E. C. OLSON[4]
Department of Astronomy, University of Illinois, Urbana, IL 61801
Received 1997 May 27; accepted 1997 September 29

ABSTRACT

A self-consistent, physically accurate program suite has been used in an accurate simulation of new spectroscopy and photometry of MR Cygni. Analysis of both the spectroscopic and photometric data used spectrum synthesis techniques and a synthetic photometry augmentation of a light synthesis program package. The theoretical light curves closely fit the observational data. The same self-consistent parameters from the light synthesis solution produced synthetic spectra precisely fitting the observed spectra at all orbital phases.

The IRAF-reduced spectroscopy has produced an accurate double-lined radial velocity curve. The derived mass ratio differs greatly from photometric mass ratios in the literature. New *UBV* photometry closely replicates existing data and indicates photometric stability of the binary system. A synthetic spectrum fitted to *IUE* data established the primary component $T_{\rm eff}$. The light curve solution determined a single set of system parameters used to calculate *U*, *B*, and *V* light curves. We conclude that MR Cygni is a member of the relatively rare class of hot Algol systems defined by Popper. It is likely that mass transfer still is in progress, but there is no evidence, either from orbital period variation or from a bright spot on the mass gainer, for its existence. The lack of Hα emission in any of our spectra, including one at phase 0.063, suggests a small current rate of mass transfer. The fact that our computationally self-consistent procedure has successfully represented both the photometry and the spectroscopy for a binary system whose components are appreciably distorted demonstrates the overall power of the procedure.

Subject headings: binaries: eclipsing — stars: individual (MR Cygni) — stars: mass loss — ultraviolet: stars

1. INTRODUCTION

MR Cygni (BD +47°3639; SAO 051509, $P = 1\overset{d}{.}7$) has been the subject of repeated photometric analyses, beginning with the classic study by Wilson & Devinney (1971; hereafter WD). The most recent analysis is by Linnell & Kallrath (1987; hereafter LK). LK include a discussion of earlier solutions. The LK solution left several system properties uncertain or poorly determined. Without accurate radial velocity curves for the two components, the LK solution depended on a photometric mass ratio. (For consistency with most of the discussions, the quoted mass ratio, *q*, is $\mathcal{M}_2/\mathcal{M}_1$, with $\mathcal{M}_2$ the less massive component. Primary minimum corresponds to a deep but partial transit eclipse of the more massive primary component.) The LK simplex solution obtained a value of $q = 0.74$, but iteration on a synthetic light curve modulated by simulated observational error produced *q* values that wandered in the range 0.69–0.82. It was possible to obtain a solution with near–main-sequence components, but alternative approaches to the character of the secondary component produced inconsistent results.

Hill & Hutchings (1973b; hereafter HH) obtained a single-component radial velocity curve for the primary, classified as B3 V. They remark on the effects of component distortion on the determination of radial velocities, and, from line strengths and line blends, find a weakly determined mass ratio $q = 0.55$. From their earlier photometric solution (Hill & Hutchings 1973a), HH determined slightly evolved but near–main sequence locations for the MR Cygni components. WD found a mass ratio of $q = 0.83$ using the double-lined radial velocity measurements by J. A. Pearce (WD) of spectra reported in Harper et al. (1935; hereafter HA), a main-sequence location for the primary, and a secondary slightly above the main sequence.

The photometric analyses all used observations by Hall & Hardie (1969; hereafter HAH). A Russell Model analysis by HAH determined main-sequence status for both components. All of the photometric analyses obtained reasonably good fits to the available photometric data. The uncertain status of this important system and the likelihood that the components lie on the main sequence made a new spectroscopic investigation, as well as new multicolor photometry, especially desirable.

A recent collaborative effort (Linnell & Hubeny 1994; hearafter LH) has developed new spectrum synthesis procedures for interacting binary stars, procedures that complement an existing light synthesis program (Linnell 1984; hereafter L84). The program package uses a single self-

[1] Visiting Scholar, Astronomy Department, University of Washington, Seattle, WA 98195; linnell@pa.msu.edu.
[2] etzel@mintaka.sdsu.edu.
[3] hubeny@stars.gsfc.nasa.gov.
[4] olsomed@sirius.astro.uiuc.edu.

TABLE 1

RADIAL VELOCITY DATA, PRIMARY COMPONENT

HJD +2,400,000.0	Phase	V_{obs} (λ4471) (km s^{-1})	V_{obs} (λ4481) (km s^{-1})	V_{cal} (km s^{-1})	$O-C$ (λ4471) (km s^{-1})	$O-C$ (λ4481) (km s^{-1})
49,993.6391	0.7799	55.7	66.2	56.1	−0.4	10.1
49,993.7925	0.8714	30.0	41.2	26.5	3.5	14.7
49,994.6092	0.3584	−145.4	−135.6	−144.5	−0.9	8.9
49,996.6133	0.5534	−27.9	−38.0	−18.4	−9.5	−19.6
49,996.6348	0.5663	−20.2	...	−9.8	−10.4	...
49,997.6032	0.1437	−144.9	−145.6	−145.4	0.5	−0.2
49,998.6265	0.7539	56.2	61.5	58.1	−1.9	3.4
49,998.6473	0.7663	57.6	64.9	57.5	0.1	7.4
49,999.6188	0.3456	−154.9	−152.3	−150.0	−4.9	−2.3
50,001.6188	0.5382	−37.6	−42.4	−28.8	−8.8	−13.6
50,002.6000	0.1233	−135.7	−139.1	−135.6	−0.1	−3.5
50,003.6042	0.7220	59.5	70.8	56.3	3.2	14.5
50,003.6243	0.7340	63.5	67.5	57.5	6.0	10.0
50,324.8056	0.2514	−167.6	...	−169.9	2.3	...
50,329.6550	0.1431	−147.3	−146.7	−145.1	−2.2	−1.6
50,329.7827	0.2193	−165.6	−156.3	−167.8	2.2	11.5
50,329.8355	0.2507	−165.6	−149.7	−169.9	4.3	20.2
50,329.8772	0.2756	−170.5	−162.5	−168.4	−2.1	5.9
50,329.9307	0.3075	−162.5	−151.5	−162.6	0.1	11.1
50,361.7210	0.2637	−164.2	...	−169.5	5.3	...
50,362.6487	0.8170	60.6	...	48.2	12.4	...

consistent model to calculate both the synthetic spectrum and the synthetic light curve. An initial application to EE Pegasi (Linnell, Hubeny, & Lacy 1996; hereafter L96) has studied a low-distortion system. As an appreciably distorted system, MR Cygni is an inviting subject for a follow-on investigation. This paper reports an application of the program suite to new spectroscopy, new *UBV* photometry, and archival *IUE* spectroscopy of MR Cygni.

2. SPECTROSCOPY

Olson & Etzel obtained a total of 28 spectra of MR Cygni at Mount Laguna Observatory (MLO) during the 1995 and 1996 observing seasons with the Illinois Cassegrain "white" spectrograph on the 1 m reflector. Spectra were obtained in the second-order blue with an 831 line mm^{-1} grating, a 38 cm focal length camera, and a liquid nitrogen–cooled TI 800 × 800 CCD. The resultant dispersion was 0.2 Å pixel^{-1} with the spectral resolution typically 0.5 Å. All but two of the spectra had exposure times of 900 s. The typical signal-to-noise ratio (S/N) in the spectrum continuum was 120. The 24 λ4471 spectra covered the interval $\lambda\lambda$4390–4564. The four Hα spectra covered the interval $\lambda\lambda$6380–6722. The calculated orbital phase values used a new initial epoch from the photometry, discussed subsequently. Standard IRAF routines were used in the reductions, performed at the University of Illinois. Lines due to the secondary are clearly visible on most of the spectra and are suitable for radial velocity measurements with a few exceptions. Radial velocities were measured by line-profile fitting on continuum-fitted spectra. The measured radial velocities of the primary component are in Table 1. Those of the secondary are in Table 2. The tabulated times of exposure and phases refer to midexposures.

The primary component radial velocities depend on measurements of both the He I λ4471 line and the Mg II λ4481 line. For the orbit solution, we assigned weights of 5.0 to the λ4471 line and 1.0 to the λ4481 line. The Mg II λ4481 line was the only secondary component line that could be measured. The primary component He I λ6678 line appeared to be measurable, but it gave discordant results and was not used in the solution. It is poorly represented in the spectrum syntheses, described subsequently. Final elements were determined by differential corrections, following the method of Léhmann-Filhes. The residuals have the following properties: primary component, s.e. (one observation) = 6.3 km s^{-1}; secondary component, s.e. (one observation) = 13.5 km s^{-1}. Table 3 lists the resulting elements. The number of velocity standards observed in 1995 were fewer than desirable; this condition makes it possible that a 1–3 km s^{-1} systematic error exists between the 1995 and 1996 data. This determined the assigned V_0 uncertainty. For reference, measurements of the radial velocity standard 10 Tau, using the same equipment as in this study, determine a value within 2 ± 2 km s^{-1} of the standard value. We believe the standard errors calculated for the K values in Table 3 are reliable.

A plot of the component radial velocities relative to the system center of mass is shown in Figure 1. The amplitudes of the theoretical radial velocity curves are given in Table 3. In the orbital phase interval 0.5–1.0, the secondary component λ4471 line is on the shortward side of the corresponding primary component line but is never displaced far enough to make it measurable. The secondary component λ4481 line merges with the broad primary component

TABLE 2

RADIAL VELOCITY DATA, SECONDARY COMPONENT

HJD +2,400,000.0	Phase	V_{obs} (λ4481) (km s^{-1})	V_{cal} (km s^{-1})	$O-C$ (km s^{-1})
49,994.6092	0.3584	188.4	165.9	22.5
49,997.6032	0.1437	169.7	168.2	1.5
49,999.6188	0.3456	199.2	179.6	19.6
50,002.6000	0.1233	117.3	143.7	−26.4
50,324.8056	0.2514	222.0	229.6	−7.6
50,329.6550	0.1431	167.9	167.5	0.4
50,329.7827	0.2193	228.6	224.3	4.3
50,329.8355	0.2507	233.2	229.6	3.6
50,329.8772	0.2756	215.7	225.9	−10.2
50,329.9306	0.3075	205.7	211.2	−5.5
50,361.7210	0.2637	226.7	228.5	−1.8

TABLE 3

MR CYGNI SYSTEM ELEMENTS, RADIAL VELOCITY SOLUTION [a]

Component	V_0 (km s^{-1})	K (km s^{-1})	$A \sin i$ (km)	$\mathcal{M} \sin^3 i$ [b]
Primary	-55.9 ± 3.0	114.0 ± 1.2	$2.629 \times 10^6 \pm 0.029 \times 10^6$	7.92 ± 0.30
Secondary.....	-55.9	285.5 ± 4.5	$6.583 \times 10^6 \pm 0.108 \times 10^6$	3.16 ± 0.08

[a] The solution was for a circular orbit with the photometric ephemeris adopted for the time of primary conjunction.

[b] Minimum masses.

λ4471 line. Consequently, radial velocity measures for the secondary component are determinable only in the phase interval 0.0–0.5.

Because our results differ greatly from earlier ones, we digress briefly to discuss previous spectroscopic studies. The earliest radial velocity study was by HA. Only spectroscopic elements were published. The derived orbital eccentricity was 0.122, based on measurements of hydrogen lines. The value of q from HA was 0.83. WD obtained J. A. Pearce's observations, used in the HA analysis, and published the double-lined radial velocity curve in the WD light synthesis paper. The radial velocity curve included values for the secondary component in the phase interval 0.5–1.0, measured by Pearce, and in contrast to our results. WD report that A. Batten stated he was unable to see lines of the secondary on his photographic spectra, and HA were also unable to identify lines for the secondary component on the same spectra. WD adopted the HA value $q = 0.83$ as a fixed parameter in their light synthesis analysis.

HAH noted that their photometry provides no indication of orbital eccentricity and that it supports the conclusion of Lavrov (1965) that the orbital eccentricity derived by HA was spurious. HAH went on to calculate that the spectroscopic orbit described by HA, together with the orbital inclination from the HAH light curve solution, leads to component masses of 3.0 $\mathcal{M}_\odot$ and 2.5 $\mathcal{M}_\odot$, far too small for stars of spectral types B3 and B8.

HH argue that the HA orbit must be rejected because it includes measurements of both hydrogen and helium lines. HH used an oscilloscope measuring device to measure plate spectra obtained in the 1930s and in 1971. They found no evidence of the secondary spectrum in their plate material. We conclude that measurements of lines for the secondary component by Pearce are spurious and that no reliable q value exists from prior spectroscopic material. In addition, since the MR Cygni system is partially eclipsing, photometric q values are unreliable (see the remarks by Rucinski 1989).

A striking result from our spectroscopy is the measured q value, 0.399 ± 0.008. We know of no larger discrepancy between spectroscopic and photometric q values based on existing photometric q values. Indeed, there was initial suspicion that something may have been wrong with our spectroscopic q value. Adoption of that value and main-sequence locations for the binary components gave unacceptably large residuals from the existing and new light curves. We were eventually driven to the recognition (see § 7) that MR Cygni is a member of the rare group of hot Algols discussed by Popper (1980, 1992). Söderhjelm (1978) reached a similar conclusion based on alternative plots of MR Cygni components in the mass-radius plane. The new radial velocity curves determine component masses of 8.0 ± 0.3 $\mathcal{M}_\odot$ and 3.2 ± 0.1 $\mathcal{M}_\odot$. The mass of the secondary component corresponds to an A0 star (Allen 1973) with a main-sequence $T_{\rm eff}$ of 9.9 kK. Our solution determines a polar $T_{\rm eff}$ of the secondary component of 13.1 kK.

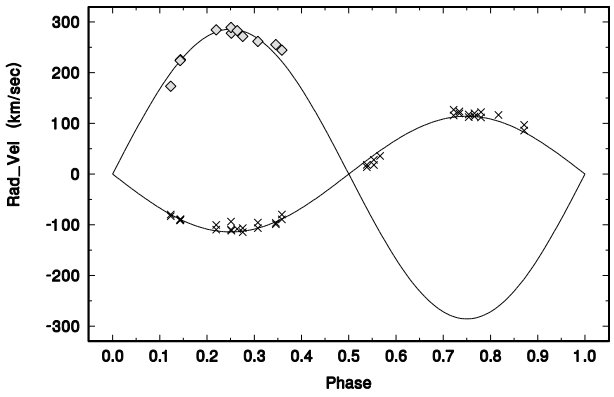

FIG. 1.—Radial velocity measurements of MR Cygni components. The crosses mark the primary component; the diamonds mark the secondary component. The theoretical radial velocity curves have amplitudes given in Table 3.

3. PHOTOMETRY

The existing photometric analyses of MR Cygni use the photometry of HAH. Independent verification of the accuracy of that data set is desirable. The HAH photometry included 343 UBV observations in each color; a substantially larger data set potentially could constrain the photometric solution more closely. The HAH photometry was done some 30 years ago, and a test is desirable to determine whether any changes in the system photometric behavior may have taken place in the interim.

UBV photometry was scheduled on the 0.6 m Smith telescope at MLO for the interval 1996 August 9–20 UT. Weather conditions permitted all-night observation of MR Cygni on 5 nights. No mid–primary minima occurred on those nights. Partial-night observations were possible on some of the other nights.

The observations included a number of Landolt standards. The primary comparison star was BD $+47°3622$ = HD 51482. The observing procedure was to integrate for 10 s separately in U, B, and V for a total of about five sets of UBV MR Cygni observations. All of the observations used a 26″ diaphragm. The objective was to achieve as large a data acquisition rate as possible. Under optimum efficiency, the five sets of observations would take of order 3 minutes. If the telescope was not too near the horizon, drift due to differential atmospheric refraction would displace the star image by less than the diaphragm radius in that time. (Fewer than five sets were observed without interruption

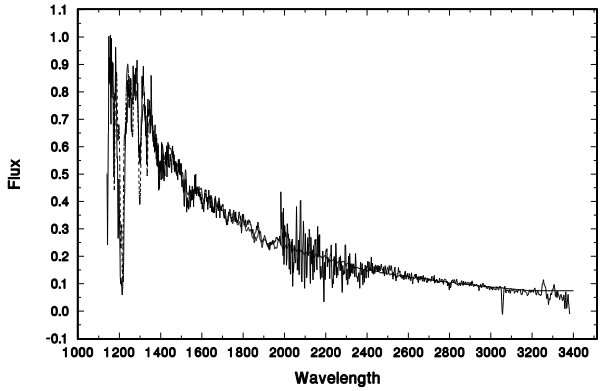

FIG. 2.—Fit of an MR Cygni synthetic spectrum to a dereddened *IUE* spectrum. This fit determines the adopted $T_{\rm eff}$ of the primary component. The feature at λ3040 is a reseau artifact. The synthetic spectrum is the heavy (*dashed*) line. Both the *IUE* and synthetic spectra have been scaled (ordinates) to superimpose the plots at approximate maximum values of 1.0.

near the horizon.) However, there was appreciable backlash in declination and it often was difficult to center the star in the diaphragm. In some instances, the reduced data disclosed that the edge of the diaphragm had begun to encroach on the star image near the end of a set of observations, particularly under conditions of bad seeing. This required deletion of some observations and further required some judgment about where in the set to start deletion.

Single sets of comparison star *UBV* observations bracketed the variable star groups. Interspersed sky observations were at approximately 0.5 hr intervals. Our comparison star (HD 51482) was the same one used for the primary comparison by HAH; their study established the photometric stability of this star. Consequently it was the only comparison star used. Photometric reductions, including transformation to the standard system defined by the Landolt standards, used the software package by Harmanec, Horn, & Juza (1994), suitably modified to accommodate more than 300 observations per night on a given object. Reduction was in differential photometry mode. Comparison star residuals from the nightly extinction lines had typical rms errors <0.015 in V and B and <0.02 in U. Use of a check star would have permitted direct determination of photometric accuracy but would have substantially reduced the data acquisition rate. After eliminating observations during deteriorating or unstable photometric conditions, the MR Cygni data set included 1503 sets of *UBV* observations. The observations of MR Cygni, transformed to the standard system, have been placed in file 326E of the Commission 27 Archives (Schmidt 1992).

A mid–secondary minimum on 1996 August 11 UT occurred at HJD 2,450,306.78055, determined by interpolation on a smooth curve through the observations over a phase interval of about 0.06 centered on the time of minimum. The HAH ephemeris predicts a corresponding time of HJD 2,450,306.78268. The descending-branch primary minimum observations of 1996 August 20 UT extended, at morning twilight, to within minutes of mid-primary minimum. These data together determine a new primary minimum ephemeris of

$$\text{Primary Minimum} = \text{HJD } 2{,}450{,}314.3217 + 1.6770343E\ .$$

The ephemeris includes a slightly adjusted orbital period. To within the data accuracy, the orbital period has remained constant since discovery.

4. THE POLAR $T_{\rm eff}$ OF THE PRIMARY COMPONENT

The primary component dominates the system spectrum in the $\lambda\lambda$1200–2000 region. Archival *IUE* spectra are available for MR Cygni in pairs of SWP and LWP exposures. The pair SWP28677 and LWP08626 was dereddened by choosing successively larger $E(B-V)$ values until, by visual estimate, the λ2200 interstellar absorption feature had been removed and the two spectra combined smoothly. Extinction correction used the standard Galactic average law of Savage & Mathis (1979). The adopted $E(B-V)$ value was 0.2. As a first approximation, synthetic spectra were calculated with program SYNSPEC (Hubeny, Lanz, & Jeffery 1994) for a succession of $T_{\rm eff}$ values and log g of 4.0. The SYNSPEC program used Kurucz LTE model atmospheres (Kurucz 1979) as input. These spectra were subjected to synchronous rotational broadening with the Hubeny program ROTINS and then compared with the dereddened *IUE* spectra. This comparison established a provisional $T_{\rm eff}$ of the primary component. Using the provisional value, the L84 program produced a light synthesis solution for the polar $T_{\rm eff}$ of the secondary. The LH program then was used to calculate a system synthetic spectrum at the orbital phase of the *IUE* spectra that could be compared to the *IUE* spectra. The resulting synthetic spectrum was convolved with a FWHM 5 Å instrument broadening function prior to comparison with the *IUE* spectra. The fit is excellent and requires no further adjustment of the primary component polar $T_{\rm eff}$ of 21.0 kK. Variation of $T_{\rm eff}$ over the primary component photosphere is relatively small. Figure 2 shows the fit of the synthetic system spectrum to the dereddened *IUE* spectra. No special processing was performed to fit the Lyα line. The accuracy of the $T_{\rm eff}$ value depends on the visual test used in the dereddening procedure. We estimate an accuracy of ± 0.5 kK.

5. LIGHT SYNTHESIS ANALYSIS AND SYNTHETIC PHOTOMETRY

The L84 program as originally developed used the Planck law to represent the radiation characteristics of stars. As discussed in L96, this representation can be seriously in error. An improved procedure in LH represents the stellar radiation characteristics by synthetic spectra. However, this procedure still calculates monochromatic light curves appropriate to the effective wavelengths of the color filters in use. Synthetic photometry (Buser & Kurucz 1992) closely duplicates the actual observing process and achieves $U-B$ and $B-V$ residuals of order 0.01 mag. In this procedure, the calculated photometric quantity is the integral of the product of the filter transmission function and the emergent flux for a particular model atmosphere. Application of this procedure to the binary star case is complicated by the fact that light intensities toward the observer, not just flux values, must be known to permit calculation of a synthetic system spectrum. Integration over the projected visible areas of the components, multiplied by the local light intensities toward the observer, produces flux values for the synthetic system spectrum. An option in SYNSPEC permits calculation of continuum intensities as well as continuum fluxes. (The calculated continuum

includes explicit calculation of absorption lines due to H and He.) This option avoids the requirement for line lists to calculate detailed spectra and permits a fast calculation of continuum intensities over a sufficiently wide wavelength range to encompass all of the UBV bandpasses. Calculated $U-B$ and $B-V$ colors with SYNSPEC flux data for individual Kurucz model atmospheres give excellent agreement (differences of order 0.01 mag) with corresponding colors from Buser & Kurucz (1992) for the $T_{\rm eff}$ range of interest for MR Cygni. We attribute the residuals to the slight contrast between our flux calculation procedure and that of Buser & Kurucz (we explicitly include H and He lines) or to differences in the details of the integration procedure. We have implemented a program that calculates synthetic UBV photometry for binary stars; a detailed description will appear elsewhere.

We emphasize that it is a *synthetic spectrum* calculation that determines the *light* values used in the light curve solution. Moreover, the evaluation of light intensities occurs at each tabular wavelength, at a spacing of 1 Å in the present instance, so that the synthetic photometry in effect determines exact limb-darkening values at 1 Å steps over the range from λ3000 to λ7000, required because of the total wavelength span of the V, B, and U filters, repeated for each fiducial orbital longitude. There is an intimate interdependence between the spectrum synthesis calculation and the light synthesis algorithm. The parameters from the light synthesis solution are needed to permit calculation of a synthetic spectrum.

The optimization process held q at the spectroscopically determined value of 0.399 and fixed the polar $T_{{\rm eff},h}$ at the value 21 kK from the fit to the IUE spectrum. We also maintained the secondary component Roche potential at the critical value to fill its Roche lobe. The final adjustments varied Ω_h, i, and $T_{{\rm eff},c}$. Note that, for physical self-consistency, L_h and L_c are calculated quantities and are not independent optimizable parameters. Bolometric albedos and gravity-brightening exponents were assigned their theoretical values for radiative envelopes (see Table 4). Limb-darkening values are not free parameters; they are exact values from synthetic spectra data, appropriate to the local conditions on the component photospheres, and are available at each computed wavelength.

The differential corrections program that includes synthetic photometry in the iterative loop requires about 3 hr per iteration on a 200 Mhz Pentium Pro PC. The reason for the long calculation time is the requirement to calculate a synthetic flux spectrum extending from λ3000 to λ7000 at each of the 49 adopted fiducial orbital longitudes for each iteration. Our optimized system parameters are in Table 4. A_h and A_c are bolometric albedos, b_h and b_c are gravity-brightening exponents, and F_h and F_c are rotation parameters, each defined as the ratio of the solid body rotation rate of the component in question to the synchronous rate. Ω_h and Ω_c are photospheric Roche potentials. Note that the $T_{{\rm eff},h}$ values specify the experimental uncertainty in their determination, although the values were fixed during the optimization process.

The V observed and theoretical (synthetic photometry) light curves are in Figure 3. The data covering the phase range 0.1–0.2 come entirely from the night of 1996 August 12 UT. The beginning of the gradually increasing residuals in all three colors approximately coincides with reversal of the telescope. It therefore is uncertain whether the departure from the theoretical curve is intrinsic to the star. The data for the phase range 0.45–0.63 come entirely from the night of 1996 August 11 UT. Again in this case, the gradually increasing residuals after phase 0.55 approximately

TABLE 4

MR CYGNI SYSTEM PARAMETERS, PHOTOMETRIC SOLUTION[a]

Parameter	Value
q	0.399 (fixed)
Ω_h	3.301 ± 0.006
r_h(pole)	0.3421 ± 0.0007
r_h(point)	0.3674 ± 0.0009
r_h(side)	0.3525 ± 0.0008
r_h(back)	0.3607 ± 0.0009
r_h(equiv.)	0.3529 ± 0.0008
log g_h(pole)	4.033 ± 0.002
log g_h(point)	3.895 ± 0.003
log g_h(side)	3.981 ± 0.002
log g_h(back)	3.940 ± 0.002
Ω_c	2.677 (fixed)
r_c(pole)	0.2824
r_c(point)	0.4069
r_c(side)	0.2944
r_c(back)	0.3270
r_c(equiv.)	0.3146
log g_c(pole)	3.817
log g_c(point)	−9.847
log g_c(side)	3.745
log g_c(back)	3.550
i (deg)	85.36 ± 0.06
A_h	1.0 (fixed)
A_c	1.0 (fixed)
b_h	0.25 (fixed)
b_c	0.25 (fixed)
F_h	1.0 (fixed)
F_c	1.0 (fixed)
$T_{{\rm eff},h}$(pole)(K)	21,000 ± 500
$T_{{\rm eff},h}$ (point) (K)	19,391 ± 500
$T_{{\rm eff},h}$ (side) (K)	20,376 ± 500
$T_{{\rm eff},h}$ (back) (K)	19,910 ± 500
$T_{{\rm eff},c}$ (pole)(K)	13,079 ± 20
$T_{{\rm eff},c}$ (point) (K)	14,839 ± 20
$T_{{\rm eff},c}$ (side) (K)	12,550 ± 20
$T_{{\rm eff},c}$ (back) (K)	11,215 ± 20
L_h/L_c (5500 Å)	2.937
L_h/L_c (4400 Å)	3.154
L_h/L_c (3650 Å)	5.131

[a] The listed errors assume an exact value for q.

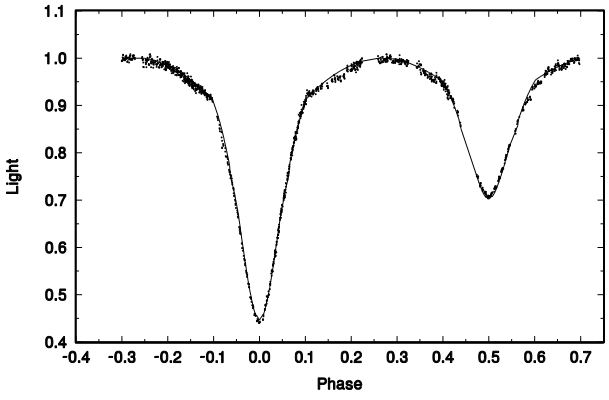

FIG. 3.—MR Cygni V synthetic light curve, using synthetic photometry, compared with photometric data from Mount Laguna Observatory.

coincide with reversal of the telescope. In both cases, the seeing deteriorated toward the end of the observing session and there were increasing instances of observations near the end of a group that had to be rejected because of obvious encroachment by the edge of the diaphragm. It is possible that the seeing was sufficiently bad to have affected the observations over an appreciable phase range. Rather than eliminate entire segments of the light curve, we have retained the data in question with the reservation that the systematic departures may not be intrinsic to the star. The V, B, and U residuals are in Figures 4, 5, and 6, respectively. Note that these are individual residuals, not normal points. Some additional discrepant points could have been eliminated but a conservative test was adopted. The standard deviations of the residuals from the theoretical light curves are: V, 0.0073; B, 0.0072; and U, 0.0098 (light units for single observations).

The use of synthetic photometry has nearly eliminated the usual discrepancy between the fit to the U light curve and fits to the V and B light curves with a given set of system parameters. The slight systematic trend in the residuals in the immediate vicinity of phase 0.0 most likely arises from a slight inaccuracy in the temperature calibration of the primary component. A contributory effect may arise from our use of a Hamamatsu R943-02 photo-

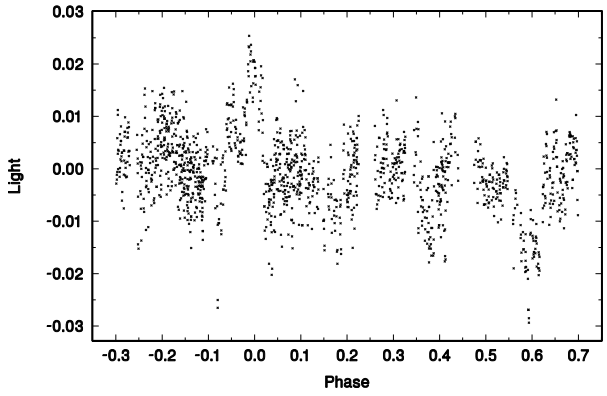

FIG. 4.—Residuals from the fit of the V synthetic light curve to photometry of Fig. 3. The data set consists of 1503 individual observations. The standard deviation of the residuals is 0.0073 (light units).

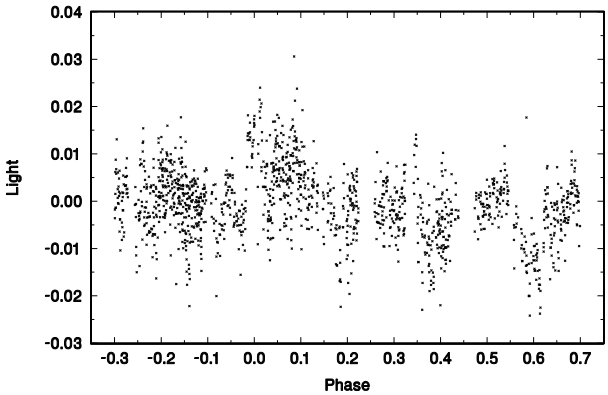

FIG. 5.—Residuals from the fit of the B synthetic light curve to photometric data from Mount Laguna Observatory. The data set consists of 1503 individual observations. The standard deviation of the residuals is 0.0072 (light units).

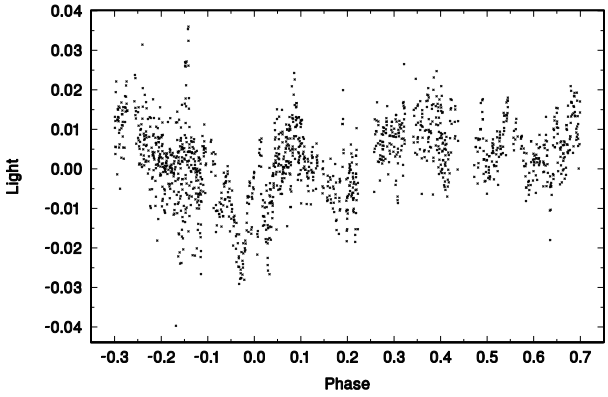

FIG. 6.—Residuals from the fit of the U synthetic light curve to photometric data from Mount Laguna Observatory. The data set consists of 1503 individual observations. The standard deviation of the residuals is 0.0098 (light units).

multiplier that, combined with our color filters, gives a color response slightly different from the response curves used by Buser (1978) in determining transformations to a standard photometric system. There is not a constant color transformation offset for the entire light curve because of the system color change during eclipses. The simultaneous least-squares solution in all three colors achieves the best possible overall fit. To gain perspective on the improvement achieved with our synthetic spectra plus synthetic photometry procedure, as compared with a solution using monochromatic Planck-law light curves, we retained the current system parameters and calculated UBV residuals from a monochromatic Planck-law representation. The U residuals remained comparable with those in Figure 6, but both the V and B residuals showed trends in opposite directions at primary and secondary minima, with peak-to-peak amplitudes of 0.07 light units.

The secondary fills its Roche lobe. This situation, together with the theoretical gravity-brightening exponent, produces a $T_{\mathrm{eff},c}$ in the absence of irradiation, of 5 K for the secondary component point that essentially coincides with the L1 point. (This temperature indicates only how closely the Roche potential of the secondary photosphere matches the critical potential; the temperature of the point in question would be 0.0 K for an exact match.) *With* irradiation, as shown in Table 4, the point T_{eff} is 14.8 kK. The basic model must break down in the point region. Our procedure calculates local T_{eff} values according to the equation

$$T_{\mathrm{eff}}^4 = T_{\mathrm{eff,inner}}^4 + (A/\sigma)F_{\mathrm{irr}} ,$$

where F_{irr} represents the flux locally incident from the companion, σ is the Stefan-Boltzmann constant, A is either A_h or A_c, and $T_{\mathrm{eff,inner}}$ is the local effective temperature in the absence of irradiation, calculated from the equation

$$T_{\mathrm{eff,inner}}(\theta, \phi) = T_{\mathrm{eff,inner}}(0, 0)[g(\theta, \phi)/g(0, 0)]^b ,$$

where θ and ϕ are colatitude and longitude, respectively, $g(0, 0)$ is the polar gravity, and b is either b_h or b_c. The resulting grid of photospheric T_{eff} values is then used to calculate interpolated spectra that sum to produce the component synthetic spectrum (via program ACPGF6, discussed subsequently). Work is in progress on relaxing this approximation and computing the model atmospheres, with irradiation, exactly by TLUSTY (Hubeny 1988). This

improvement will eliminate the need for bolometric albedos.

We have given some thought to the accuracy of our system parameters. We believe formal values of parameter standard deviations, from the off-diagonal elements of a least-squares solution matrix, often understate the uncertainty of the parameters. Popper (1984) suggests multiplying formal errors from least squares by a factor of 3 to provide more realistic measures of uncertainty. The photometric residuals, as is true in the present case, may not have a normal distribution. Having found a minimum variance, we performed an additional differentials correction calculation for simultaneous variation of i, Ω_h, and $T_{\rm eff,c}$(pole). We then arbitrarily doubled the calculated uncertainties of those parameters for entry in Table 4. Note that the listed uncertainty for $T_{\rm eff,c}$ assumes an exact value for $T_{\rm eff,h}$(pole). [As already mentioned, the estimated uncertainty in $T_{\rm eff,h}$(pole) comes from the fit of the synthetic system spectrum to the dereddened *IUE* spectrum.] The values of L_h/L_c are from the theoretical light curves at orbital longitude $\pi/2$ and include effects of irradiation. The secondary component fills its Roche lobe. Varying the secondary component Roche potential to produce successively larger amounts of underfill produced successively larger photometric residuals. Overplotting the HAH data on the new MLO photometry demonstrated consistency of the two data sets as precise as could be determined by visual examination. The HAH data show appreciable scatter in the phase range between 0.1 and 0.2, and there are only three data points in the phase interval 0.6–0.7. Consequently, no comparative statement can be made concerning the residuals trends in our data, in those phase intervals, and those in the HAH data. The major discrepancy between our system parameters and those of earlier studies working with comparable data sets serves to emphasize the inherent indeterminacy of photometric solutions of partially eclipsing systems.

6. SPECTRUM SYNTHESIS

LH demonstrated that, at an S/N of 200, a detectable difference would exist between a synthetic spectrum for a single model atmosphere and a synthetic spectrum allowing for variation of $T_{\rm eff}$ and log g over the photospheres of the small distortion system EE Pegasi. With the appreciably greater distortion of its photospheres, the MR Cygni components require the spectrum synthesis procedures described in LH and L96.

The system parameters of Table 4 provide the basic information to calculate synthetic spectra. Program ACPGF6 calculates synthetic spectra for the binary system. The procedure is discussed in L96. That paper refers to program ACPGF2, an early version of ACPGF6. ACPGF6 inputs a group of reference synthetic spectra for each of the binary components. The reference spectra, calculated with SYNSPEC, pertain to model atmospheres with specified values of $T_{\rm eff}$ and log g chosen so that they bracket the ranges of those parameters over the stellar photospheres. SYNSPEC used a line list for a restricted spectral interval to limit the required computer time. For example, the synthetic spectra fitting the He I λ4471 line used a line list for the interval $\lambda\lambda$3400–5000.

ACPGF6 also inputs data for each surface element on the photospheres of both binary components. The data include local values of $T_{\rm eff}$, log g, radial velocity, element visibility to the observer, cos γ (where γ is the angle between the local surface normal and the line of sight to the observer), and projected area. ACPGF6 then calculates the contribution of each photospheric element to the spectrum of the binary components separately, as well as the composite system spectrum. ACPGF6 takes into account the variation of $T_{\rm eff}$ and log g over the photospheres as well as Doppler effects due to rotation and orbital motion. The input reference spectra include effects of other line-broadening mechanisms. Different values of orbital inclination and orbital longitude modify the second data set to ACPGF6.

In the present instance, ACPGF6 used reference spectra of $T_{\rm eff}$ = 19 kK, 20 kK, and 21 kK and log g = 4.0 for the primary component and of $T_{\rm eff}$ = 11 kK, 12 kK, 13 kK, and 14 kK and log g = 4.0 for the secondary component. (We neglected the effect of variable gravity over the photospheres on the spectra.) It is useful to reemphasize that ACPGF6 is part of the loop of successive programs for both the detailed synthetic spectra and synthetic photometry. Light intensities are required in both cases. In the first case, the source synthetic spectra input to ACPGF6 include the full complement of absorption lines calculated by SYNSPEC with a line list. In the second case, the source synthetic spectra are continuum values, also calculated by SYNSPEC, and include lines for H and He explicitly provided in the SYNSPEC program.

We present a comparison of synthetic spectra with observational data for orbital phases 0.2193, 0.7663, 0.5382, and 0.9634, respectively, in Figures 7, 8, 9, and 10. The phases listed for the synthetic spectra refer to the midphase of the corresponding exposure. These are a representative sample from fits to all 28 observed spectra. The fits were accomplished by dividing the theoretical flux values by a normalization constant and applying a straight line rectification correction for the slope of the theoretical continuum. The Doppler effect from orbital motion of the primary is evident by comparison of the λ4471 line with the abscissa scale.

The presence of the secondary is clear in an examination of the He I λ4471 line, the Mg II λ4481 line, and the Si III

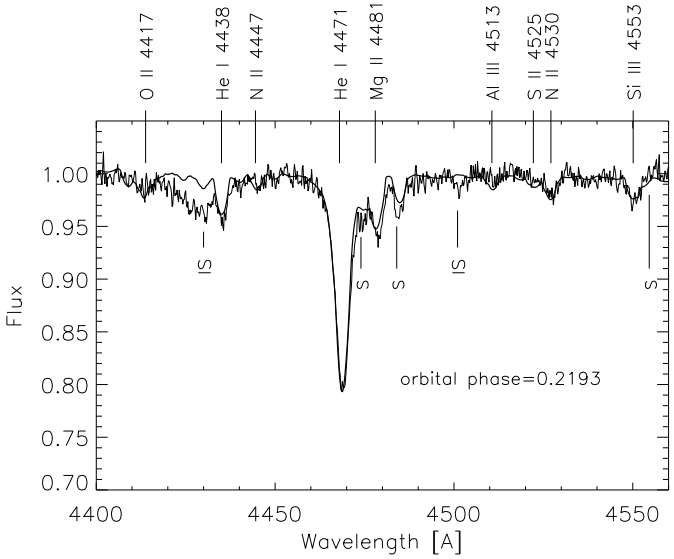

FIG. 7.—Fit of synthetic system spectrum to observed spectrum at orbital phase 0.2193. The thin line is the observed spectrum; the thick line is the synthetic spectrum. The positions of the diffuse interstellar bands are marked "IS," and the lines of the secondary component are marked "S."

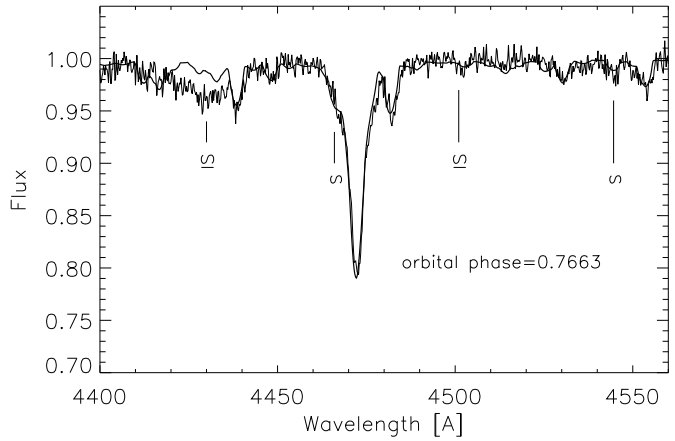

FIG. 8.—Fit of the synthetic system spectrum to the observed spectrum at orbital phase 0.7663. Identifications and line thicknesses are as in Fig. 7.

λ4553 line in Figures 7 and 8. Except for the diffuse interstellar bands at λ4430 and λ4501 (Puget & Legér 1989), the fit of the synthetic spectra to the observed spectra is excellent. In particular, note the deepening of the λ4471 line at secondary eclipse in Figure 9. That line is shallower for the secondary component, relative to the secondary component continuum, than is the case for the primary. Outside eclipse, the contribution of the secondary tends to fill in the absorption line, making it shallower relative to the system continuum. This feature, in addition to the photometric depth of secondary minimum, provides a control on the polar $T_{\rm eff}$ of the secondary component. A larger secondary $T_{\rm eff}$ produces a greater fractional contribution to the system spectrum and so produces a shallower predicted primary component λ4471 line. The calculated strength of the λ4471 line includes the forbidden component as well as the permitted components. The forbidden component makes a detectable contribution.

Since the absorption-line equivalent widths are temperature sensitive, the excellent fit of the synthetic spectra to the MLO data, together with the fit to the *IUE* spectra, provide strong evidence in support of the adopted system parameters. This point receives further support from the fit of the synthetic spectra to the Hα line in Figure 11, showing orbital phases 0.1996 and 0.7954. The secondary component contribution is apparent on opposite sides of the primary component line. (The HAH comment about the Pearce radial velocity measurements is strongly echoed in Fig. 11.) In addition, there are primary component contributions from C II λ6578 and C II λ6583. The He I λ6678 line also is prominent. The failure to fit this line is well known in synthetic spectrum studies and remains unexplained.

The spectra are consistent with synchronous rotation. The absorption-line depths are sensitive to the rotation parameter. A faster than synchronous rotation quickly reduces the absorption-line depths and produces a discrepancy with observations. Although secondary component

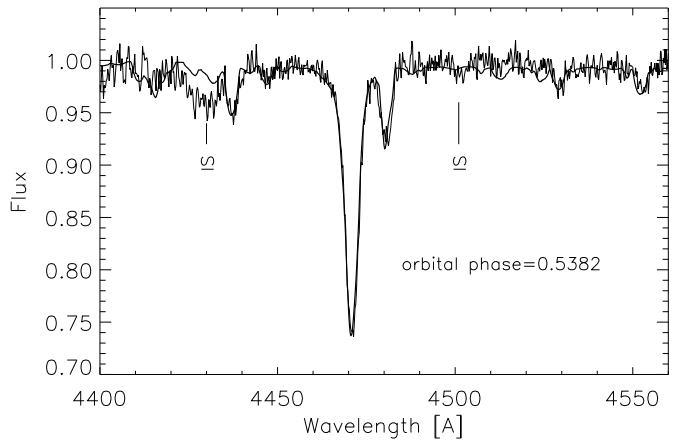

FIG. 9.—Fit of the synthetic system spectrum to the observed spectrum at orbital phase 0.5382. Identifications and line thicknesses are as in Fig. 7.

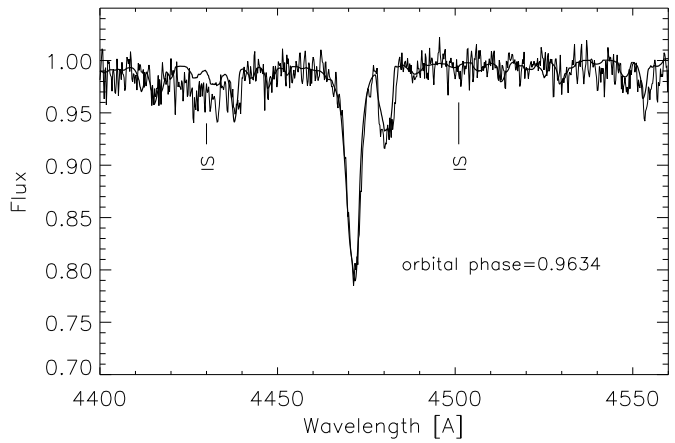

FIG. 10.—Fit of the synthetic system spectrum to the observed spectrum at orbital phase 0.9634. Identifications and line thicknesses are as in Fig. 7.

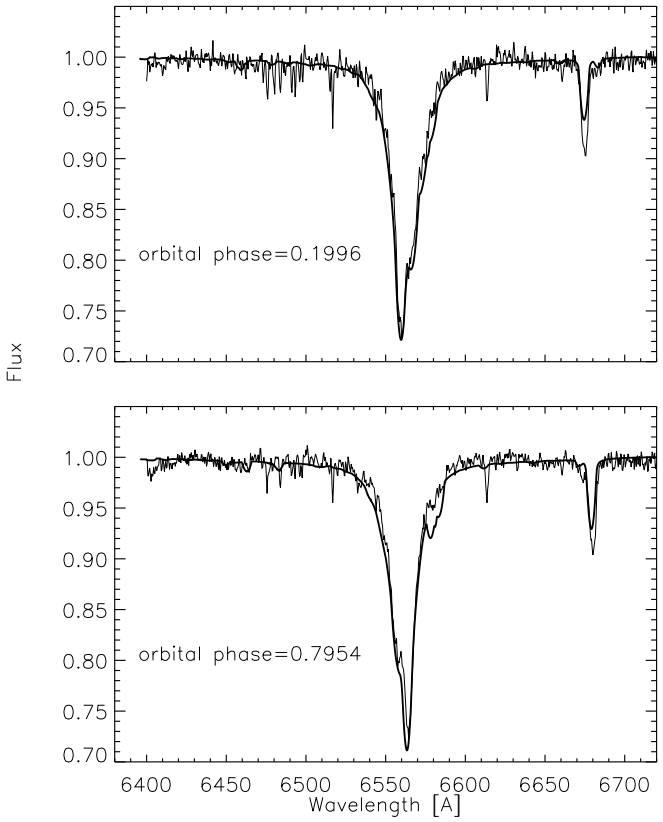

FIG. 11.—Fit of the synthetic system spectrum to the observed Hα spectrum at orbital phases 0.1996 and 0.7954. In addition to the Hα line, the He I λ6678 line is visible. Note the line asymmetry produced by the contribution of the secondary component.

radial velocities were measurable only for the Mg II λ4481 line and for a limited phase interval, that line and other secondary component lines clearly are present in the data for additional phase intervals, as the fit of the synthetic spectra makes evident.

It is important to recognize that the fit of our synthetic spectra to the observed spectra involves *no individual parameter adjustments* other than application of a normalization factor for vertical superposition and a rectification factor made necessary because the observational data are rectified. Once the system parameters are determined by light synthesis analysis, the assignment of only an orbital longitude, together with our spectrum synthesis algorithm, produces a synthetic spectrum that fits the observational data with excellent precision. Yet the light synthesis analysis uses theoretical light values that result directly from a spectrum synthesis procedure for the continuum flux, together with synthetic photometry. The light synthesis and spectrum synthesis algorithms are intimately connected, mutually interdependent computational procedures. This combined computational structure is our most important result.

We believe it likely that a sensitive procedure for radial velocity measurements could be developed based on our synthetic spectra algorithm. However, extensive testing and calibration would be needed, including application to a variety of synthetic and real binary star systems.

7. DISCUSSION AND CONCLUSIONS

The system absolute elements are in Table 5. The component separation followed from the K and corresponding $A*$ sin i values of Table 3 and the i value of Table 4. In calculating A and its error, the values of K_h and K_c (Table 3) first were set at their best values, then K_h at its extreme, and then K_c at its extreme. The larger error was retained. The errors in the absolute radii assume a linear worst case sum of the error contributions from the component separation and the fractional radii of Table 4. The sum of the masses follows from the $A * \sin i$ values of Table 3, the i value of Table 4, and Kepler's law, with no error assumed for sin i in its product with the sum of the masses. The individual masses then followed from the spectroscopic mass ratio. Errors in the masses followed from the final column of Table 3 together with the value of i from Table 4. The log $T_{\rm eff}$ ("equiv.") entries reference the (isothermal) blackbody boundary temperature of a sphere of surface area equal to the component in question and radiating a total luminosity equal to that emerging from the interior. The reradiated energy incident from the companion is excluded. The same condition applies to the bolometric and V magnitudes and to the component luminosities. Note that the entries in Table 4 include the effects of irradiation. The component radii, shown in Table 5, are the radii of spheres with volumes equal to the (distorted) component volumes. Given the values of L_h, L_c, and $M_{V,h}$, the system $M_V = -2.2(2)$. The photometric reductions determine a maximum light value of $m_V = 8.82$. With $A_V = 0.66$ [using the estimated $E(B-V)$ from the *IUE* spectrum fit], the distance to MR Cygni is 1200 pc. We estimate an uncertainty of 100 pc. The cool component radii in Tables 4 and 5 have no uncertainties listed because the component fills its Roche lobe.

TABLE 5

MR CYGNI ABSOLUTE PARAMETERS

Parameter	Value
A ($R_\odot$)	13.24 ± 0.17
log L_h ($L_\odot$)	3.54 ± 0.04
log $T_{\rm eff,h}$ (equiv.)	4.31 ± 0.01
$M_{V,h}$	−2.1 ± 0.1
$M_{\rm bol,h}$	−4.1 ± 0.1
$\mathcal{M}_h$ ($\mathcal{M}_\odot$)	8.00 ± 0.30
R_h (equiv.) ($R_\odot$)	4.67 ± 0.07
ρ_h (mean)	0.11
d (pc)	1200 ± 100
log L_c ($L_\odot$)	2.52 ± 0.02
log $T_{\rm eff,c}$ (equiv.)	4.09 ± 0.01
$M_{V,c}$	−0.9 ± 0.1
$M_{\rm bol,c}$	−1.6 ± 0.1
$\mathcal{M}_c$ ($\mathcal{M}_\odot$)	3.19 ± 0.08
R_c (equiv.) ($R_\odot$)	4.17
ρ_c (mean)	0.07

Superposition of HAH data and the new photometry shows precise concordance, as well as can be determined by visual estimate, and indicates long term photometric stability. This result contrasts with those for other Algol systems, such as AQ Cas (Olson 1994), UX Mon (Olson & Etzel 1995), or KU Cyg (Olson, Etzel, & Dewey 1995). On the other hand, S Cnc (Olson & Etzel 1993), like MR Cygni, shows photometric stability. The fact that the mass loser in AQ Cas has a radiative envelope, as does the MR Cygni mass loser, argues against photometric stability being a simple consequence of a radiative envelope for the lobe-filling component.

Binary star evolution codes indicate that Algols are still in the mass transfer phase of their evolution (De Greve & de Loore 1992; de Loore & Doom 1992, p. 355). The evolution model for a $9\,\mathcal{M}_\odot + 5\,\mathcal{M}_\odot$ system (de Loore & Doom 1992, p. 342) may be roughly representative of MR Cygni. In that case, MR Cygni has recently entered the phase of slow mass transfer, with a transfer rate of order $10^{-8}\,\mathcal{M}_\odot\ {\rm yr}^{-1}$. This transfer rate, if conservative, would produce a period increase in 50 yr that would barely affect the seventh decimal of the orbital period. However, it is likely that the gainer has mass loss via a wind (Chiosi & Maeder 1986) that may be comparable within an order of magnitude with the mass transfer stream. The wind would tend to counteract the effect of the mass transfer stream. The uncertainties are sufficient that the lack of an observed period change provides no evidence for or against the existence of a slow mass transfer. The lack of Hα emission in any of our spectra, including one at phase 0.063, is a direct indication of a small current rate of mass transfer (see Fig. 11).

The radius of the primary is large enough that a mass transfer stream would impact the primary directly rather than form an accretion disk (Lubow & Shu 1975). It would seem reasonable to expect a bright spot at the impact point of the mass transfer stream, yet there is no photometric evidence for a bright spot. Olson (1980) argues that the ram pressure of the incoming stream may lead to dissipation of the liberated energy below the photosphere in the case of U Cep; a similar process may be in operation in MR Cygni. Based on the fit of solar composition synthetic spectra to the limited span of the MLO spectra, there is no evidence for abundance anomalies.

Figure 12 shows a Hertzsprung-Russell diagram for binary components from the lists of Popper (1980) and Andersen (1991). Components from Popper's lists of detached and visual binary systems are marked with crosses; those from Andersen's list are marked by dots. The

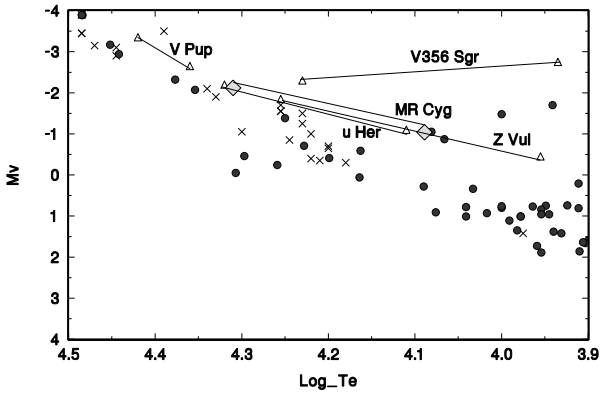

FIG. 12.—Hertzsprung-Russell diagram showing the locations of MR Cygni components (*diamonds*). Other hot semidetached systems show as triangles, which are connected by lines and labeled. Binary components from lists of Popper appear as crosses, and binary components from the list of Andersen appear as dots. For clarity, the line joining the u Herculis components has been placed at the bottom of the component triangles, and the line joining the MR Cygni components has been placed at the top of the component diamonds.

components of Popper's hot Algol group are designated by triangles. Diamonds mark the locations of the MR Cygni components. The MR Cygni components nearly duplicate the components of the u Herculis system.

There are two considerations that drove us to classify MR Cygni as an Algol system. First, the spectroscopic mass ratio is a high-weight determination, while a photometric mass ratio is essentially indeterminate for a partially eclipsing system. However, adoption of the spectroscopic mass ratio, together with the large photometric ellipticity, implies a secondary component of small relative mass that occupies a large volume, an object unlike a near–main-sequence star. Assumed main-sequence locations for the two components produces light curves totally unlike those observed. Second, adopting the spectroscopic mass ratio produces a photometric solution that precisely fits photometric data and leads to components that are both understandable in terms of stellar evolution and are similar to those of other known stars.

The fact that our computationally self-consistent procedure has successfully represented both the photometry and the spectroscopy for a binary system whose components are appreciably distorted demonstrates the overall power of the procedure.

The conclusions of this study are the following:

1. Previous studies of MR Cygni derived system parameters that were inaccurate, largely because of the basic photometric indeterminacy of a partially eclipsing system together with a poorly known mass ratio.
2. MR Cygni is one of the hot Algol systems and likely has recently entered the slow phase of mass transfer following mass reversal.
3. This system likely contains a mass transfer stream but direct evidence for its existence is lacking.
4. A self-consistent physical model has been used, together with an integrated, interdependent computational algorithm for both spectrum synthesis and light synthesis analysis. The program output simulates both spectroscopic and photometric data for MR Cygni and achieves an excellent representation of all the data studied. This success, illustrating the power of the computational procedure, is our most significant result.

This research was partially supported by a grant from NASA administered by the American Astronomical Society and by NASA grant NAG 5-3484 to A. P. L.; P. B. E. acknowledges support under NSF grant AST 94-17035. A. P. L. thanks the director of Mount Laguna Observatory for a generous grant of observing time and P. Harmanec for use of the Ondrejov photometric reduction package. We thank the referee for useful criticisms.

REFERENCES

Allen, C. W. 1973, Astrophysical Quantities (3rd ed.; London: Athlone)
Andersen, J. 1991, A&A Rev., 3, 91
Buser, R. 1978, A&A, 62, 411
Buser, R., & Kurucz, R. L. 1992, A&A, 264, 557
Chiosi, C., & Maeder, A. 1986, ARA&A, 24, 329
De Greve, J. P., & de Loore, C. W. H. 1992, A&AS, 96, 653
de Loore, C. W. H., & Doom, C. 1992, Structure and Evolution of Single and Binary Stars (Dordrecht: Kluwer)
Hall, D. A., & Hardie, R. H. 1969, PASP, 81, 754 (HAH)
Harmanec, P., Horn, J., & Juza, K. 1994, A&AS, 104, 121
Harper, W. E., Pearce, J. A., Petrie, R. M., & McKellar, A. 1935, JRASC, 29, 411 (HA)
Hill, G., & Hutchings, J. B. 1973a, Ap&SS, 20, 123
———. 1973b, A&A, 23, 357 (HH)
Hubeny, I. 1988, Comput. Phys. Commun., 52, 103
Hubeny, I., Lanz, T., & Jeffery, C. S. 1994, in Newsl. Anal. Astron. Spectra 20, ed. C. S. Jeffery (St. Andrews: St. Andrews Univ.), 30
Kurucz, R. L. 1979, ApJS, 40, 1
Lavrov, M. I. 1965, Bull. Engelhardt Obs. 38
Linnell, A. P. 1984, ApJS, 54, 17 (L84)
Linnell, A. P., & Hubeny, I. 1994, ApJ, 434, 738 (LH)
Linnell, A. P., Hubeny, I., & Lacy, C. H. S. 1996, ApJ, 459, 721 (L96)
Linnell, A. P., & Kallrath, J. 1987, ApJ, 316, 754 (LK)
Lubow, S. H., & Shu, F. H. 1975, ApJ, 198, 383
Olson, E. C. 1980, ApJ, 241, 257
———. 1994, AJ, 108, 666
Olson, E. C., & Etzel, P. B. 1993, AJ, 106, 1162
———. 1995, AJ, 110, 2385
Olson, E. C., Etzel, P. B., & Dewey, M. R. 1995, AJ, 110, 2378
Popper, D. M. 1980, ARA&A, 18, 115
———. 1984, AJ, 89, 132
———. 1992, in IAU Symp. 151, Evolutionary Processes in Interacting Binary Stars, ed. Y. Kondo, R. F. Sistero, & R. S. Polidan (Dordrecht: Kluwer), 395
Puget, J. L., & Léger, A. 1989, ARA&A, 27, 161
Rucinski, S. 1989, in Algols, ed. A. H. Batten (Dordrecht: Kluwer), 326
Savage, B. D., & Mathis, J. S. 1979, ARA&A, 17, 73
Schmidt, E. G. 1992, Inf. Bull. Variable Stars 3773
Söderhjelm, S. 1978, A&A, 66, 161
Wilson, R. E., & Devinney, E. J. 1971, ApJ, 166, 605 (WD)